Journal of Zhejiang University-SCIENCE A 2026 27(1):58-75
www.jzus.zju.edu.cn; www.springer.com/journal/11582
E-mail: jzus_a@zju.edu.cn

Research Article
https://doi.org/10.1631/jzus.A2400413

Check for updates

Optimal hierarchical control of speed and energy usage for hybrid ships considering navigational environment

Zhe XIONG[1,2,3], Yupeng YUAN[1,2,3]✉, Liang TONG[1,2,3], Jianshu CHU[4], Boyang SHEN[5]

[1]*State Key Laboratory of Maritime Technology and Safety, Wuhan University of Technology, Wuhan 430063, China*
[2]*National Engineering Research Center for Water Transport Safety (WTS Center), Wuhan University of Technology, Wuhan 430063, China*
[3]*Reliability Engineering Institute, School of Transportation and Logistics Engineering, Wuhan University of Technology, Wuhan 430063, China*
[4]*COSCO Shipping Heavy Industry Co. Ltd., Shanghai 200135, China*
[5]*Department of Engineering, University of Cambridge, Cambridge CB3 0FA, UK*

Abstract: The concept of hybrid ships has gained significant attention in recent years, as they offer an effective means of enhancing energy utilization and reducing environmental pollution. However, the navigational environments of ships are often subject to changes, which in turn affect their energy efficiency in a complex manner. It is therefore evident that enhancing the energy efficiency of hybrid ships is a worthwhile goal. In this study, we take a diesel-electric hybrid ship navigating in inland waterways as the research object, and propose a hierarchical optimization method for ship energy efficiency. The upper-layer control establishes a predictive model for propulsion motor speed and fuel consumption through multivariate time series predictions, and employs the model predictive control (MPC) method to optimize the propulsion motor speed. The lower-layer control utilizes an equivalent fuel consumption minimization method, which is based on improving the equivalence factor. This involves combining the variation of the supercapacitor's state of charge (SOC) with the propulsion motor speed obtained from the MPC optimization in the upper-layer control. Furthermore, a proportional integral (PI) controller is used to adjust the equivalence factor, in order to adapt the equivalent fuel consumption minimization method to the working conditions. Our results demonstrate that the proposed hierarchical optimization method can reduce the energy efficiency operating indicator (EEOI) by approximately 11.54% and the fuel consumption by approximately 9.47% in comparison to the pre-optimization scenario.

Key words: Equivalent fuel consumption minimization strategy; Energy efficiency optimization; Operating condition adaptation; Hybrid ships

1 Introduction

Fossil fuels have been the primary energy source for maritime vessels for over a century, and over 80% of global trade is reliant on shipping (UNCTAD, 2022). However, combustion of these fuels has increased greenhouse gas (GHG) emissions, contributing to severe environmental pollution (Liu et al., 2018). To address this, the Marine Environment Protection Committee (MEPC) of International Maritime Organization (IMO) adopted the 2023 IMO GHG Strategy, aiming for widespread adoption of low-GHG fuels by 2030, and net-zero emissions from international shipping by 2050 (IMO, 2023).

In recent years, the power sources of ships have diversified, leading to so-called hybrid ships. These can overcome the limitation of using a single energy source by comprehensively utilizing renewable energy sources, such as mechanical energy, electrical energy, hydrogen energy, and solar energy (Sulligoi et al., 2016; Hein et al., 2021). In order to reasonably manage the coupled system of multiple power sources, it is necessary to formulate appropriate energy management strategies that distribute the output power or torque of each power source, coordinate mechanical propulsion and electric propulsion, and ensure the safe supply of power to the ship (Balsamo et al., 2017). Currently, energy management strategies for hybrid ships can be classified into three categories according to different theories and methodologies: rule-based

✉ Yupeng YUAN, ypyuan@whut.edu.cn
Yupeng YUAN, https://orcid.org/0000-0001-9474-0605

Received Aug. 24, 2024; Revision accepted Mar. 17, 2025;
Crosschecked Oct. 30, 2025; Online first Nov. 29, 2025

energy management strategies, optimization-based energy management strategies, and learning-based energy management strategies (Han et al., 2020). The classification of these different strategies and typical algorithms associated with them are shown in Fig. S1 of the electronic supplementary materials (ESM).

Among these methods, the rule-based control strategy is relatively simple to implement and has a low operating workload. Zhu et al. (2014) designed an energy management strategy based on fuzzy control, and simulated and tested the strategy under various operating conditions for a hybrid ship utilizing fuel cells, batteries, and supercapacitors. The results showed that this strategy enabled the supercapacitors to bear more dynamic loads, thereby adjusting the operating range of the fuel cell and improving the system's energy efficiency. Khan et al. (2017) used a fuzzy control algorithm to enable the energy storage battery and supercapacitor of an all-electric ship system to cooperate, so as to cope with peak and pulse loads, and maintain stable and efficient operation. Learning-based control strategies usually make use of the nonlinear modeling and predictive capabilities of neural networks, and are applied in fields such as route planning, speed prediction, and parameter optimization. Hasanvand et al. (2020) proposed a cost-effective optimal energy scheduling scheme, which approaches load loss expectation and cost minimization as a multi-objective optimization problem, and employs a deep Q-network to establish the energy management strategy. Experimental results showed that this method is more cost-effective than the traditional rule-based method, and can reduce the load expectation index. Wu et al. (2020) modeled the optimal energy scheduling problem of a plug-in hybrid fuel cell ship as a Markov decision process, and applied a double-Q learning algorithm for training; their simulation results showed that this method could achieve a similar effect to the dynamic planning method.

Real-time optimized energy management strategies such as the equivalent consumption minimization strategy (ECMS) and model predictive control (MPC) are more accurate than rule-based methods, in addition to having a clearer calculation framework and lower computational cost than learning-based methods (Guo et al., 2017). Kalikatzarakis et al. (2018), Zahedi et al. (2014), and Bassam et al. (2017) studied multi-energy hybrid systems on ships, established a minimum instantaneous equivalent fuel consumption model for hybrid power systems, and used software to calculate the fuel economy of hybrid power systems using actual ship operating parameters. Their results demonstrated that the minimum instantaneous ECMS has advantages in improving the energy efficiency of hybrid ships.

The equivalence factor in the ECMS strategy uniformly quantifies electricity and fuel consumption by converting battery or supercapacitor energy use into an equivalent diesel fuel consumption. It represents fuel consumption per unit of electrical energy, enabling a unified optimization framework to assess energy efficiency and guide optimization strategies.

Current research on equivalence factors focuses on identifying the current working conditions of the ship and determining the optimal equivalence factor under the current working conditions through optimization algorithms. By considering ultracapacitor's state of charge (SOC) and propulsion power demand, this method can optimize energy distribution. When SOC is low, the factor increases to conserve power, and when SOC or engine load is high, the factor decreases to boost supercapacitor discharge, stabilizing the engine load. This adaptive mechanism improves energy efficiency and responsiveness to changing navigation conditions. To this end, Tian et al. (2020) proposed an adaptive equivalent fuel consumption minimization strategy and constructed a fuzzy inference system that generates optimal equivalence factors in real time. Verification through simulations showed that the fuel economy of this strategy was better than that of other strategies. Zhu et al. (2020) proposed a modified adaptive equivalent consumption minimization strategy (MAECMS), which is based on ECMS. It determines the equivalence factor online by identifying the status of the power equipment based on current or predicted information, and reduces the amount of calculation by extending the optimization time step and establishing constraints. Xie et al. (2021) proposed a real-time power management strategy based on ECMS and MPC for the on-board power system of hybrid electric ships. This strategy can dynamically adjust the power distribution between the diesel generator and the hybrid energy storage system, to achieve real-time load tracking and minimize fuel consumption while adjusting the equivalence factor through MPC; in this way, it improves the adaptability and efficiency of the system. Liu et al. (2021) developed an energy control

strategy for hybrid electric ships based on an ECMS, and achieved power balance and fuel economy optimization of the power battery by adjusting the efficiency factor and its correction function.

However, ships are often in a dynamically changing navigational environment during their operation, and not in an ideal static state. Complex and shifting conditions, such as wind speed, water flow, and load, will constantly alter the operating conditions of the ship, making the equivalence factor calculated by traditional optimization algorithms only accurate at the current time step; this may lead to lagging or mismatching of the energy distribution during actual navigation, thus affecting the fuel economy and maintenance of the battery SOC.

In view of the above problems, it is urgent to develop a dynamic adjustment mechanism for the equivalence factor that can adapt to dynamic changes in working conditions, so as to achieve efficient instantaneous optimization and improve the adaptive energy distribution in complex navigation environments. To this end, we propose a hierarchical optimal control method for ship speed and energy management that accounts for the navigation environment. The method aims to improve the overall fuel economy of the ship. In the upper layer of the optimization, environmental factors such as wind speed, wind direction, water depth, and water current speed during navigation are comprehensively considered. A radial basis function (RBF) neural network is used to predict the propeller motor speed and fuel consumption, and the MPC method is used to optimize the propeller motor speed in the time domain. In the lower-level optimization, an equivalence factor adjustment strategy based on a proportional integral (PI) controller is designed according to the dynamic changes in the propeller motor speed and the SOC of the supercapacitor, and the adaptability of the ECMS to changing working conditions is optimized. An adaptive ECMS (A-ECMS) methodology for working conditions is accordingly proposed.

This paper is structured as follows. Section 2 introduces the longitudinal dynamics model and the power system model for a hybrid ship. Section 3 presents a hierarchical optimization and control model based on the navigational environment, including an upper speed optimization model and a lower energy management strategy model. In Section 4, we test the approach on a case study. The final section gives conclusions.

2 Mathematical modeling

In this paper, a hybrid electric propulsion ship traveling between Yichang and Chongqing in China is taken as the object of study. The sailing route of the ship is shown in Fig. S2 of the ESM, and a schematic diagram of the power system is shown in Fig. 1. The power source of the ship is comprised of four 1250 kW diesel engine sets, two sets of 300 kW supercapacitors, and two 1680 kW propulsion motors, with the specific parameters shown in Table 1.

The ship energy management system optimizes energy allocation and fuel economy through four key models. The diesel generator model links output power to fuel consumption. The supercapacitor model regulates energy output to stabilize load fluctuations and enhance the dynamic response. The propeller model defines power transfer, thrust, and efficiency constraints for propulsion optimization. The drag model simulates total resistance to refine the propulsion power calculations. Together, these models enable real-time optimization and efficient operation in complex navigational conditions.

2.1 Ship power system modeling

2.1.1 Diesel generator unit modeling

The manifold absolute pressure (MAP) diagram shown in Fig. 2 was obtained by conducting experimental tests on the genset to record the fuel consumption at different rotational speeds and loads.

Based on the MAP diagram, the corresponding diesel engine specific fuel consumption b_e can be determined from rotational speed and torque:

$$b_e = f(N_e,\ T_e), \tag{1}$$

where N_e indicates the rotational speed of the diesel engine, r/min; T_e indicates the diesel engine torque, N·m.

From Eq. (1), the diesel engine fuel consumption is derived as follows:

$$\dot{m}_e = \frac{b_e \cdot P_e}{3600}, \tag{2}$$

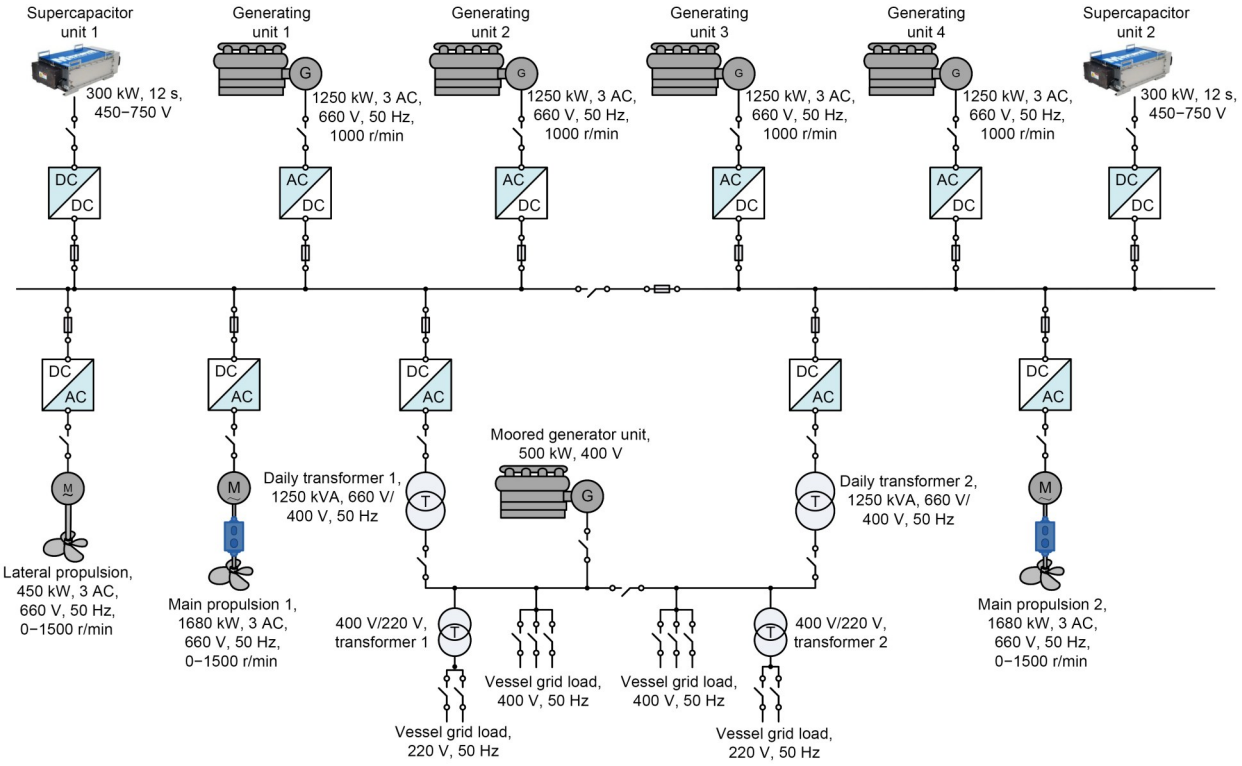

Fig. 1 Topology of the hybrid power system of the target vessel. AC: alternating current; DC: direct current

Table 1 Main parameters of the target vessel power system

Component	Basic parameter	Value
Diesel engine unit	Maximum power (kW)	1320
	Rated power (kW)	1250
	Number of units	4
Generating unit	Rated power (kW)	1250
	Rated rotational speed (r/min)	1000
	Rated voltage (AC) (V)	660
	Number of units	4
Supercapacitor unit	Single rated capacity (F)	64.5
	Single rated power (kW)	300
	Working voltage (DC) (V)	604–820

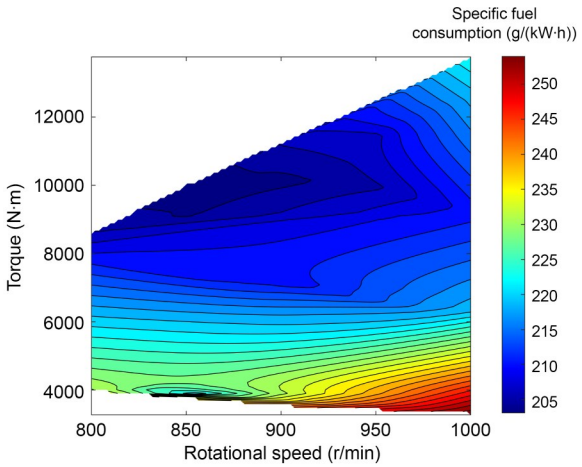

Fig. 2 MAP diagram of the diesel generator unit

where $\dot{m}_e$ is diesel fuel consumption per unit of time, g/s; P_e is the diesel engine output power, kW.

The overall output power of the diesel generator is then:

$$P_f = P_e \cdot \eta, \tag{3}$$

where P_f is the diesel generator output power, kW; η is the generator efficiency.

2.1.2 Supercapacitor modeling

The output power of the supercapacitor is given by:

$$P_{sc} = U_{sc} I_{sc} - I_{sc}^2 R_{sc}, \tag{4}$$

where P_{sc} is the supercapacitor output power, kW; U_{sc} is the supercapacitor terminal voltage, V; I_{sc} is the

supercapacitor current, A; R_{sc} is the supercapacitor internal resistance, Ω.

The SOC (S_{OC}) of the supercapacitor can be calculated from

$$S_{OC}=\frac{U_{sc}-U_{sc\_min}}{U_{sc\_max}-U_{sc\_min}}, \tag{5}$$

where U_{sc_max} is the maximum operating voltage of the supercapacitor, V; U_{sc_min} is the minimum operating voltage of the supercapacitor, V.

The equation for supercapacitor current can be derived from Eq. (5) as follows:

$$I_{sc}=\frac{U_{scmm}S_{OC}-\sqrt{U_{scmm}^2-4P_{sc}R_{sc}}}{2R_{sc}}, \tag{6}$$

where U_{scmm} is the difference between the maximum and minimum voltages of the supercapacitor, V.

2.1.3 Ship propulsion system modeling

2.1.3.1 Propeller propulsion modeling

The torque T_p and thrust T_{h_p} of the propeller are the key parameters describing its hydrodynamic performance. The equations defining them are as follows (Hou et al., 2018):

$$T_{h\_p}=K_T D_p^4 \rho \cdot N_p^2, \tag{7}$$
$$T_p=K_Q D_p^5 \rho \cdot N_p^2, \tag{8}$$

where ρ denotes the density of river water, kg/m^3; N_p denotes the rotational speed of the propeller; D_p denotes the diameter of the propeller, m; K_T and K_Q denote the thrust and torque coefficients of the propeller, respectively. K_T and K_Q are typically determined by fitting the experimental data from the ship model.

2.1.3.2 Gearbox modeling

From the propeller model, drag model, and vessel power system mechanism, the torque T_p and speed N of the reduction gearbox output can be determined, and then by using the characteristics of the speed gearbox itself, the rotational speed and torque of the motor output can be determined:

$$T_m=\frac{T_p}{\tau}, \tag{9}$$

$$N_m=N\cdot\tau, \tag{10}$$

where T_m denotes the input torque of the reduction gearbox (and also the output torque of the propulsion motor), N·m; τ denotes the runtime, s; N_m denotes the input rotational speed of the reduction gearbox (and also the output rotational speed of the propulsion motor), r/min.

2.2 Ship resistance modeling

As shown in Fig. 3, the vessel propeller generates a thrust T_{h_p}, which overcomes the total resistance R_{total} to propel the vessel forward. According to the principle of longitudinal vessel dynamics, the force on the target vessel satisfies the following equation (Geertsma et al., 2017; Carlton, 2018):

$$n_p T_{h\_p}(1-t_1)-R_{total}=ma, \tag{11}$$

where n_p is the number of propellers; t_1 is the propeller thrust deduction coefficient; m is the vessel mass, kg; a is the vessel acceleration, m/s^2.

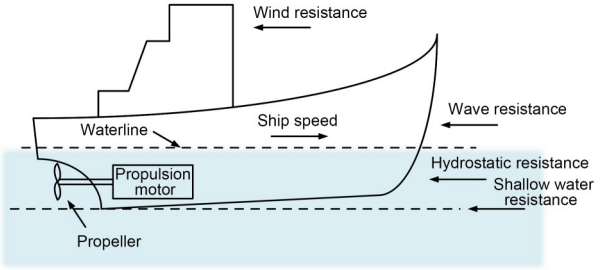

Fig. 3 Schematic diagram of the ship force analysis

As can be seen from Fig. 3, the total resistance R_{total} during ship navigation is divided into hydrostatic resistance and resistance generated by the navigational environment. The total hydrostatic resistance R_{static} can be determined by the Holtrop and Mennen (1982), and the resistance generated by the navigational environment includes the shallow water drag R_s, wind drag R_{wind}, and wave drag R_{wave}, which satisfy:

$$R_{total}=R_{static}+R_s+R_{wind}+R_{wave}. \tag{12}$$

Holtrop's method considers that the total hydrostatic resistance of a ship can be expressed by the following equation (Holtrop and Mennen, 1982; Holtrop, 1984):

$$R_{\text{static}} = R_{\text{F}}(1+k_1) + R_{\text{APP}} + R_{\text{W}} + R_{\text{B}} + R_{\text{TR}} + R_{\text{A}}, \quad (13)$$

where R_{F} is the ship's friction force, N; $1+k_1$ is the ship's viscous drag factor; R_{APP} is the appendage drag, N; R_{W} is the wave-breaking drag, N; R_{B} is the additional drag near the water surface at the bow bulb, N; R_{TR} is the additional pressure drag of the square stern when submerged, N; R_{A} is the relevant drag of the model-ship conversion, N.

In order to ensure that the ship can move forward normally, the required power P_{req} of the ship during navigation can be determined by the following formula:

$$P_{\text{req}} = R_{\text{total}} \cdot V_{\text{s}} + P_{\text{day}} = 2P_{\text{f}} + P_{\text{sc}}, \quad (14)$$

where V_{s} denotes the ship speed relative to water; P_{day} is the daily load of the ship, kW. When the ultracapacitor bank is in a charging state, $P_{\text{sc}}<0$, and when the ultracapacitor bank is in a discharging state, $P_{\text{sc}}>0$.

3 Optimal hierarchical control model for ships based on their navigational environment

We structure the control model into four key modules, as shown in Fig. 4: MPC optimization, resistance and power calculation, PI control, and A-ECMS control. The MPC module uses navigation data and an RBF neural network to predict and adjust propeller speed N in real time, so as to minimize the energy efficiency operating indicator (EEOI). The resistance and power module calculates demand based on ship and environmental factors, providing input for energy distribution. The PI control module adjusts the equivalence factor using SOC feedback to improve system

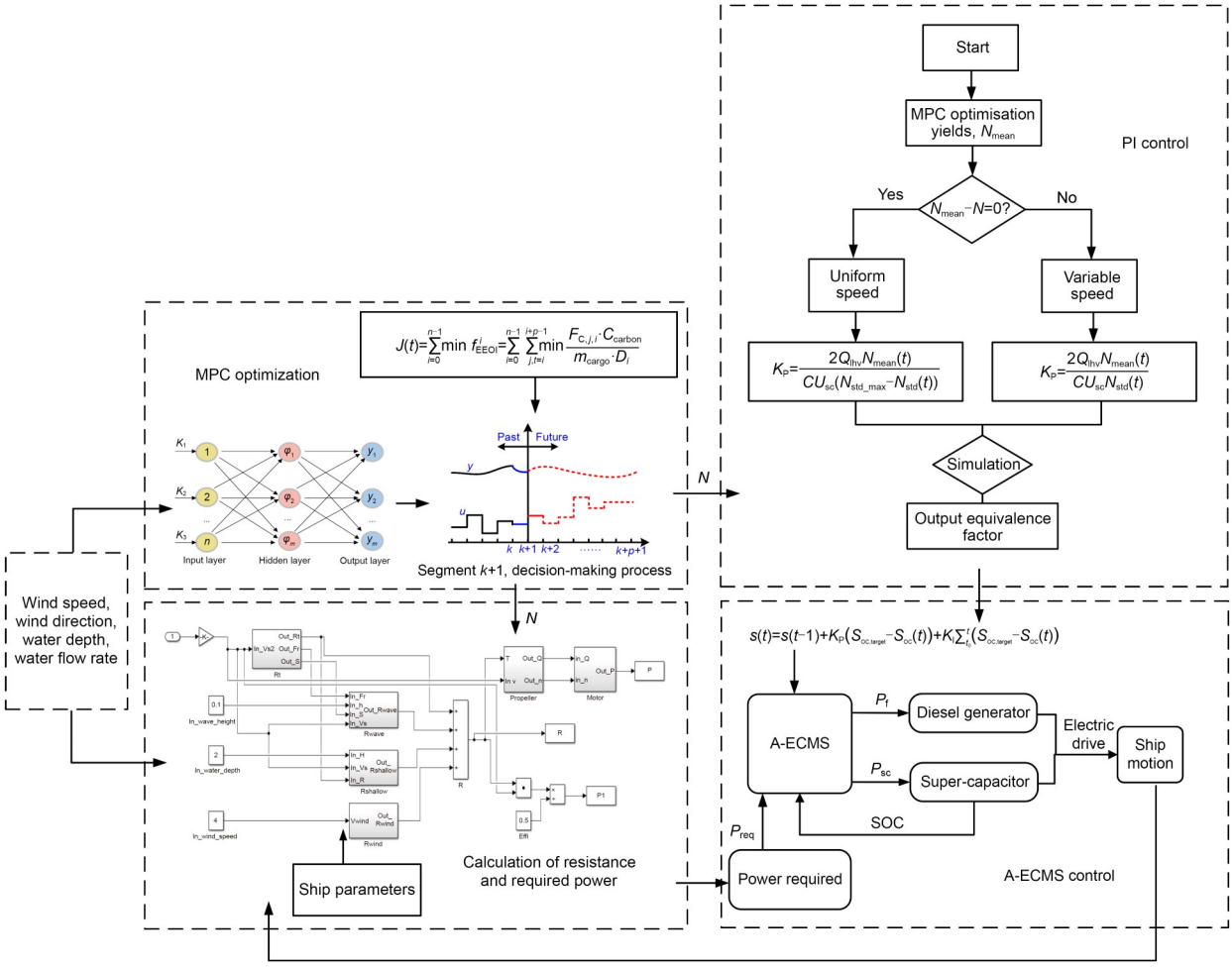

Fig. 4 Control modeling flowchart. The variables are explained in the main text

stability. The A-ECMS module optimizes energy distribution between the diesel generator and supercapacitor for precise propulsion control and improved fuel efficiency. These modules cooperate to enhance adaptability, improve energy efficiency, and reduce fuel consumption.

3.1 Upper deck speed optimization model based on navigational environment

3.1.1 RBF-based multivariate time series prediction model

The multivariate time-series prediction model uses historical data and multiple inputs (e.g., environmental factors, speed, and fuel consumption) to forecast future speed and fuel use, thus enhancing the reliability of the MPC optimization.

This study presents the use of an RBF network for the establishment of a multivariate time series prediction model. RBF networks have powerful mapping capabilities, which can effectively fit the effects of nonlinear factors (such as wind speed, waves, and water flow speed) on the rotational speed and fuel consumption in ship propulsion systems. Compared with auto-regressive integrated moving average (ARIMA) and long short-term memory (LSTM) networks, RBF networks have higher training efficiency, stronger generalization ability, and lower training data requirements, and are particularly suitable for real-time prediction scenarios. In addition, their structure being based on the Gaussian function facilitates analysis of the impact of input variables on system performance, so they have straightforward physical interpretability and application advantages. The RBF network is a feed-forward neural network comprising three principal layers: the input layer, the hidden layer, and the output layer (Hou et al., 2021; Gao et al., 2024).

The RBF network learns the mapping between the input data and the output data by adjusting the number of neurons in the hidden layer and the center and diffusion factor of each neuron, as shown in Fig. 5.

In practice, the prediction of ship fuel consumption is contingent upon not only the navigational environment, but also the predicted value of the propulsion motor speed. To address this issue, a two-step prediction model is employed, as illustrated in Fig. 6. Initially, the RBF neural network prediction model is employed to forecast the ship's propulsion motor

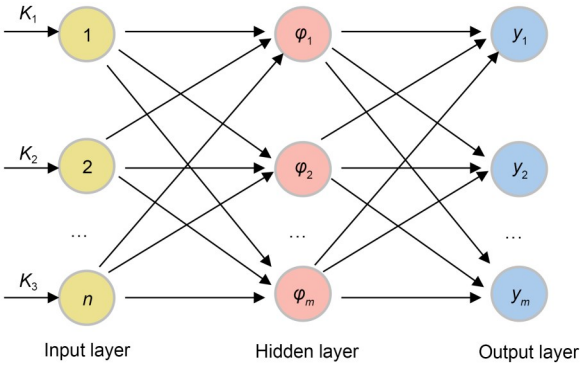

Fig. 5 Structure of the RBF neural network

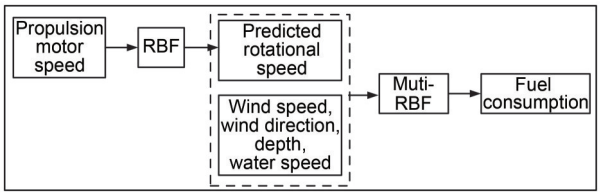

Fig. 6 Diagram of the two-step RBF prediction process

speed within a single time series. Subsequently, the ship's fuel consumption is predicted in conjunction with the navigational environment.

3.1.2 Design of the objective function for rolling optimization

The main objective of the MPC is to minimize the EEOI of the ship by optimizing the speed of the propulsion motor during ship navigation. The objective optimization function $J(t)$ is:

$$J(t)=\sum_{i=r}^{n-1}\min f_{\mathrm{EEOI}}^{i}=\sum_{i=r}^{n-1}\sum_{j,t=i}^{i+p-1}\frac{F_{\mathrm{C},j,i}\cdot C_{\mathrm{carbon}}}{m_{\mathrm{cargo}}\cdot D_i}, \quad (15)$$

where n denotes the nth rolling window; i denotes the current time step of MPC control; $\min f_{\mathrm{EEOI}}^{i}$ denotes the minimum EEOI for the vessel optimized in the ith iteration; p is the prediction step of MPC; $F_{\mathrm{C},j,i}$ denotes the total amount of j-fuel consumed by the ship in the ith prediction time domain, t; C_{carbon} denotes the carbon emission factor of diesel fuel, which is taken to be 3.11 according to IMO standards; m_{cargo} denotes the ship's load capacity during the voyage, t; D_i denotes the voyage mileage of the ith prediction time domain, km.

Combined with the diesel engine model, the ship's fuel consumption $F_{\mathrm{C},i}$ can be determined as:

$$F_{\mathrm{C},i}=\sum_{i=r}^{r+n-1} g_i(V_{i\_\mathrm{s}},\ V_{i\_\mathrm{wind}},\ \theta_{i\_\mathrm{wind}},\ H_i,\ h_i)\times \frac{D_i}{1.852(V_{i\_\mathrm{s}}+V_{i\_\mathrm{w}})}\cdot\rho_{\mathrm{d}}\times 10^{-3}, \tag{16}$$

where r denotes the rth iteration of rolling optimization; g_i denotes the fuel consumption rate of the ship during operation at the ith moment, L/h; V_{i_s} is the ship-to-water speed at the ith moment, kn (1 kn= 1.852 km/h). The ship-to-ground speed $V_{i\_\mathrm{g}}=V_{i\_\mathrm{s}}\pm V_{i\_\mathrm{w}}$, where V_{i_w} denotes the speed of the water current, kn. V_{i_wind}, θ_{i_wind}, H_i, and h_i denote the wind speed, wind direction, depth of the water, and height of the waves at the ith moment, respectively; ρ_{d} is the density of diesel fuel, which is taken to be 0.991 kg/L.

The propulsion motor speed and the ship's speed satisfy a certain functional relationship, given by:

$$V_{i\_\mathrm{s}}=f(N(t)), \tag{17}$$

where $N(t)$ denotes the speed of the propulsion motor at moment t, r/min.

By combining Eqs. (15)–(17), it can be deduced that:

$$J(t)=\min f_{\mathrm{EEOI}}^{i}=\sum_{i=r}^{n-1}\sum_{j,t=i}^{i+p-1}\frac{g_i(V_{i\_s},\ V_{i\_\mathrm{wind}},\ \theta_{i\_\mathrm{wind}},\ H_i,\ h_i)\cdot\rho_{\mathrm{d}}\times 10^{-3}\cdot C_{\mathrm{carbon}}}{1.852(f(N(t))+V_{i\_\mathrm{w}})\cdot m_{\mathrm{cargo}}}. \tag{18}$$

Ship propulsion motors have a maximum speed limit, and the speed predicted in the solution cannot exceed that value:

$$0\leqslant N(t)\leqslant N_{\max}. \tag{19}$$

As the core optimization algorithm, MPC runs throughout the entire upper-layer optimization and control process. The key feature of MPC is its rolling optimization and real-time feedback mechanism, which can continuously adjust the speeds of propulsion motors and the energy allocation strategy in a dynamic navigational environment (Li et al., 2022; Liu et al., 2023), in order to achieve instantaneous optimization and a global optimum. The entire execution process of MPC is shown in the schematic in Fig. S3 of the ESM, and its implementation includes the following stages:

(1) Prediction stage. Based on the current navigation status data, the trained RBF multivariate time series prediction model is called to predict the propulsion motor speed, fuel consumption, and range data for multiple future time steps (prediction time domain), providing predicted values for the objective function (EEOI) and laying the foundation for optimization.

(2) Optimization phase. The optimization solver is used to solve the minimization problem of the objective function, and the speed of the propulsion motor is dynamically adjusted under physical constraints (such as speed limits) to ensure that the EEOI is optimized in the predicted time domain.

(3) Execution phase. The propulsion motor speed obtained by the optimization is executed in the current control time domain, and the computational complexity of the global optimization is reduced through step-by-step execution, providing a basis for rolling window adjustment of the next time step.

(4) Feedback correction phase. The latest navigation data is collected in real time to correct the input of the prediction model and dynamically adjust the optimization path, ensuring the reliability of the objective function calculation results and adaptability of the optimization.

3.2 Optimization-based lower energy management strategies

Based on the principles of the ECMS (Chen et al., 2022), the equivalent fuel consumption function is established as:

$$\dot{m}_{\mathrm{eq}}(t)=\dot{m}_{\mathrm{f}}(t)+\dot{m}_{\mathrm{ele}}(t)=\dot{m}_{\mathrm{f}}(t)+s(t)\cdot\frac{P_{\mathrm{sc}}(t)}{Q_{\mathrm{lhv}}}, \tag{20}$$

where $\dot{m}_{\mathrm{eq}}$, $\dot{m}_{\mathrm{f}}$, and $\dot{m}_{\mathrm{ele}}$ are the instantaneous equivalent fuel consumption rates, g/(kW·h), for the ship, diesel generator set, and supercapacitor, respectively; $s(t)$ is the equivalence factor; $P_{\mathrm{sc}}(t)$ is the output power of the supercapacitor, kW; Q_{lhv} is the low calorific value of the fuel oil, 42700 kJ/kg.

In addition, the system should satisfy the following constraints:

$$\begin{cases}0<P_{\mathrm{f}}\leqslant P_{\mathrm{f\_max}},\\ 0.3\leqslant S_{\mathrm{OC}}\leqslant 0.8,\\ N_{\mathrm{e\_min}}\leqslant N_{\mathrm{e}}\leqslant N_{\mathrm{e\_max}},\end{cases} \tag{21}$$

where P_{f_max} is the maximum output power of the diesel generator, kW; N_{e_min} and N_{e_max} are the minimum and maximum rotational speeds of the diesel engine, respectively.

Pontryagin's maximum principle (PMP) is utilized to represent the value of fuel consumption as a function, and the relevant Hamiltonian function is as follows (Zhang et al., 2017):

$$H(x(t),\ u(t),\ s(t),\ t)=\dot{m}_{\mathrm{f}}(t)+\lambda(t)f(x(t),\ u(t),\ t), \quad (22)$$

where $u(t)$ is the control variable. $f(x(t),\ u(t),\ t)$ is the state transfer equation of the system given by the following expression:

$$f(x(t),\ u(t),\ t)=\dot{S}_{\mathrm{OC}}(t)=-\frac{I_{\mathrm{sc}}}{CU_{\mathrm{scmm}}}, \quad (23)$$

where $\dot{S}_{\mathrm{OC}}(t)$ is the rate of change of the supercapacitor SOC; C is the supercapacitor capacity, F.

From the Hamiltonian function, the accompanying equation is obtained:

$$\dot{\lambda}(t)=-\frac{\partial H}{\partial S_{\mathrm{OC}}}=-\lambda(t)\frac{\partial \dot{S}_{\mathrm{OC}}}{\partial S_{\mathrm{OC}}}, \quad (24)$$

where λ is the covariate.

To obtain the variable equivalence factor related to the real-time operating conditions, the concept of the SOC penalty function is introduced. The cost function $J(S_{\mathrm{OC}}(t))$ representing the supercapacitor state is redesigned as follows:

$$\begin{aligned}J(S_{\mathrm{OC}}(t))=&J_{\mathrm{f}}+J_{\mathrm{sc}}+J_{\mathrm{SOC}}=\\&\int_{t_0}^{t}\dot{m}_{\mathrm{f}}(u(t),\ t)\,\mathrm{d}t+\eta\cdot\frac{C}{Q_{\mathrm{lhv}}}\times\\&\int_{S_{\mathrm{OC}}(t_0)}^{S_{\mathrm{OC}}(t)}U_{\mathrm{sc}}\,\mathrm{d}(1-S_{\mathrm{OC}}(t))+\\&\rho_{\mathrm{p}}(S_{\mathrm{OC,target}}-S_{\mathrm{OC}}(t))^2,\end{aligned} \quad (25)$$

where J_{f}, J_{sc}, and J_{SOC} denote the costs of the diesel generator, supercapacitor, and SOC penalties, respectively; t_0 and t denote the initial and current moments, respectively; η is the ratio of the average efficiency of the engine to the average efficiency of the motor; $S_{\mathrm{OC}}(t_0)$ denotes the SOC of the supercapacitor at the initial moment; ρ_{p} is the penalty factor; $S_{\mathrm{OC,target}}$ denotes the target SOC of the supercapacitor.

According to the Hamilton-Jacobi equation, the optimal covariate expression can be obtained as:

$$\begin{aligned}\lambda^*(t)=&\frac{\partial J(S_{\mathrm{OC}}(t))}{\partial S_{\mathrm{OC}}(t)}=\\&-\eta\cdot\frac{CU_{\mathrm{sc}}}{Q_{\mathrm{lhv}}}-2\rho_{\mathrm{p}}(S_{\mathrm{OC,target}}-S_{\mathrm{OC}}(t)).\end{aligned} \quad (26)$$

In the current study, Eq. (26) is often simplified to:

$$s(t)=s_0+K(S_{\mathrm{OC,target}}-S_{\mathrm{OC}}(t)), \quad (27)$$

where s_0 is the initial value of the equivalence factor, and K is a constant factor.

In this paper, we propose a method of calculating the equivalence factor that considers the navigational environment. To facilitate simulation calculations, we discretize continuous systems while the steady state error of the system is eliminated by the PI controller, and the equivalence factor is adjusted according to the difference between the S_{OC} and $S_{\mathrm{OC,target}}$ of the supercapacitor at the current moment. The calculation of the equivalence factor is performed as follows:

$$\begin{aligned}s(t)=&s(t-1)+K_{\mathrm{P}}(S_{\mathrm{OC,target}}-S_{\mathrm{OC}}(t))+\\&K_{\mathrm{I}}\sum_{t_0}^{t}(S_{\mathrm{OC,target}}-S_{\mathrm{OC}}(t)),\end{aligned} \quad (28)$$

where K_{P} and K_{I} denote the proportional and integral coefficients of the PI control, respectively.

Accordingly, the term K_{P} is modified by the anticipated rotational velocity of the MPC, ensuring that the direction of alteration aligns with the direction of change in rotational velocity. This is calculated by Eqs. (29)–(32):

$$K_{\mathrm{P}}=\frac{2Q_{\mathrm{lhv}}N_{\mathrm{mean}}(t)}{CU_{\mathrm{sc}}N_{\mathrm{sub}}}, \quad (29)$$

$$N_{\mathrm{sub}}=\begin{cases}N_{\mathrm{std\_max}}-N_{\mathrm{std}}(t), & \text{variable-speed navigation,}\\ N_{\mathrm{std}}(t), & \text{homogeneous navigation,}\end{cases} \quad (30)$$

$$N_{\mathrm{mean}}(t)=\frac{1}{n}\sum_{t=1}^{n}N_{\mathrm{k}}, \quad (31)$$

$$N_{\mathrm{std}}(t)=\sqrt{\frac{\sum_{t=1}^{n}(N_{\mathrm{k}}-N_{\mathrm{mean}}(t))}{n}}, \quad (32)$$

where $N_{mean}(t)$ is the mean value of rotational speed predicted by the MPC at time t, r/min; N_{sub} is the intermediate variable used to distinguish between variable-speed and constant-speed operating conditions. $N_{std}(t)$ is the standard deviation of rotational speed predicted by the MPC at time t, r/min; N_{std_max} is the maximum standard deviation of the system's predicted rotational speed, r/min; n is the number of predicted rotational speed points; N_k is the value of rotational speed predicted by the MPC at time t, r/min.

4 Case study

4.1 Predictive model training

The target vessel gathers a set of operational data recorded along the route from Yichang to Chongqing, which spans approximately 550 km. The operational data from Fengdu to Chongqing is selected as the training set to train the RBF neural network prediction model. The distance between Fengdu and Chongqing is approximately 176.34 km, with a total sailing time of 28670 s. The navigational environment of this section is illustrated in Fig. 7. The figures illustrate the variations in wind speed, wind direction, water depth, and current speed across this navigation section. The maximum wind speed reached during navigation was 7.8 m/s, with significant fluctuations throughout. The wind direction varied from 30° to 90°, indicating a complex wind environment. Furthermore, the water depth exhibited a continuous variation between 10 m and 90 m, reflecting the topographic undulations in the inland waterway. In comparison, the water velocity was relatively stable, fluctuating between 1.0 m/s and 2.0 m/s. The frequent variations in these environmental parameters demonstrate that the navigational environment in this section of the route is highly complex, and rigorous navigation control is needed in order to improve efficiency.

Fig. 8 shows the historical data of the propulsion motor speed from Fengdu to Chongqing; the first 80% of the data is selected as the training set, and the last 20% of the data is selected as the test set. The numbers of input and output neurons of the RBF are set to 10, 20, and 30, respectively, the learning rate is set to 0.005, the systematic error is set to 1×10^{-5}, and the number of iterations is set to 1000. The durations of 10 s, 20 s, and 30 s were selected as the prediction

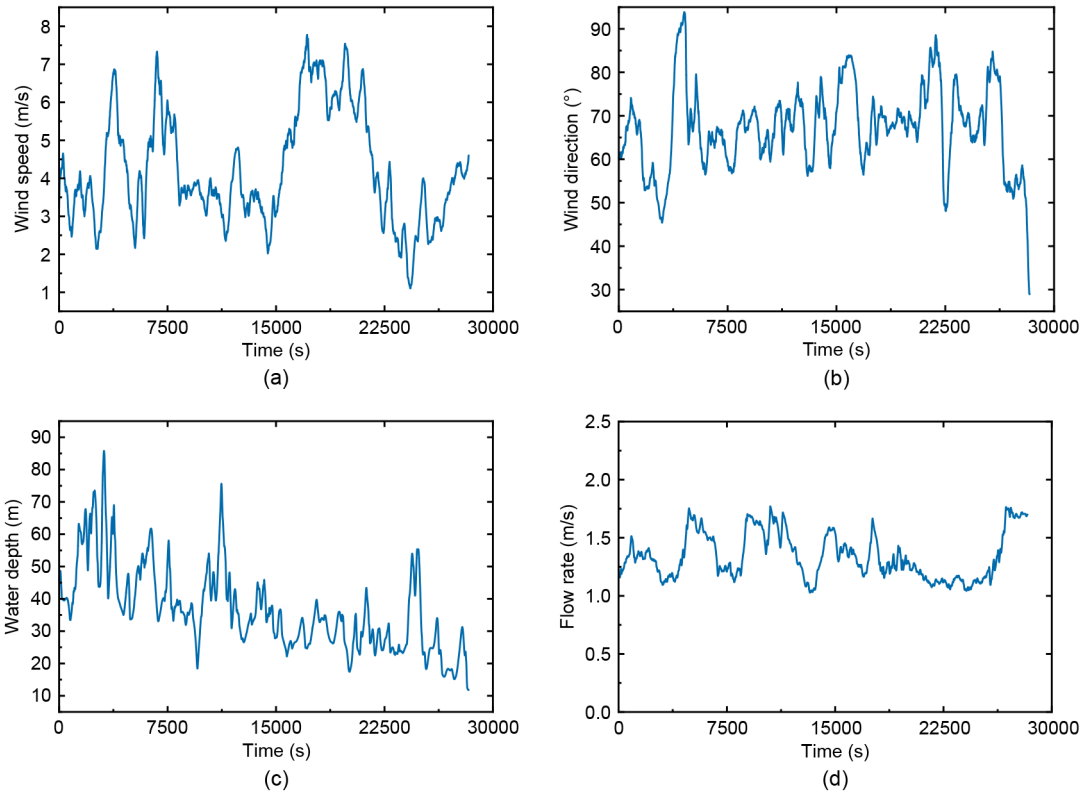

Fig. 7 Fengdu-Chongqing navigational environment: (a) wind speed; (b) wind direction; (c) water depth; (d) flow rate

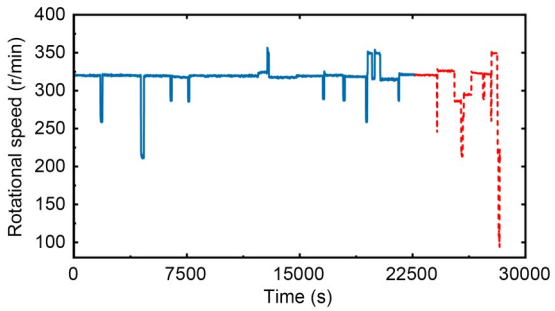

Fig. 8 Historical data of the rotational speed of propulsion motor

durations, and Fig. 9 shows the test results of the rotational speed prediction model. Comparing Figs. 9a–9c, it can be seen that under the above three prediction durations, the trends of the predicted speed and the real speed are basically the same. When the prediction time is 10 s, the trends of the predicted value and the real value are very close; when the prediction time is increased to 20 s and 30 s, the difference between the predicted value and the real value becomes larger when the rotational speed changes significantly. Therefore, in the subsequent rolling optimization process, the prediction time is chosen as 10 s and the control time as 5 s. After completing each step of optimization, the time window is rolled forward for 5 s, and the above steps are repeated until the whole rolling optimization process is completed.

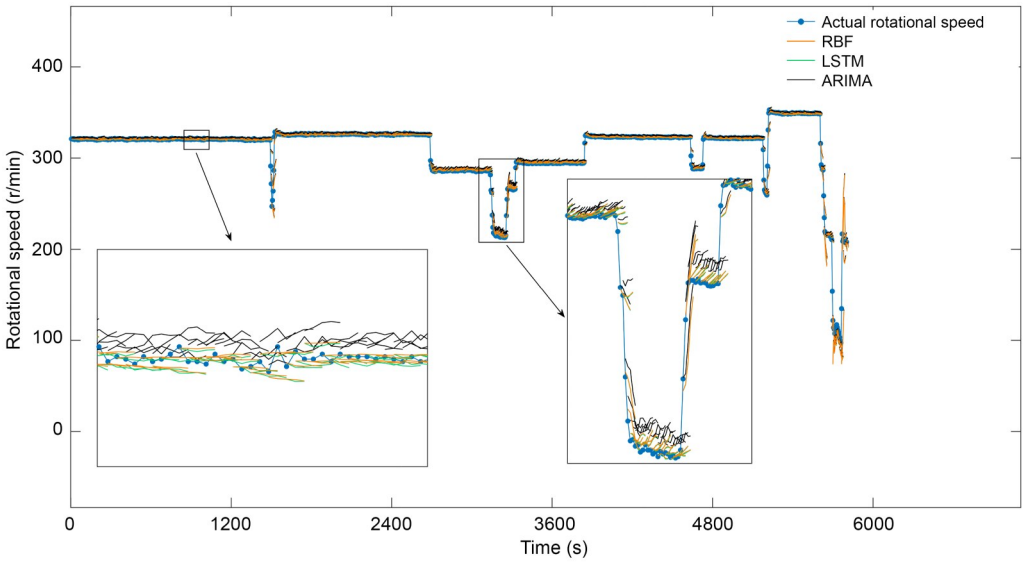

(a)

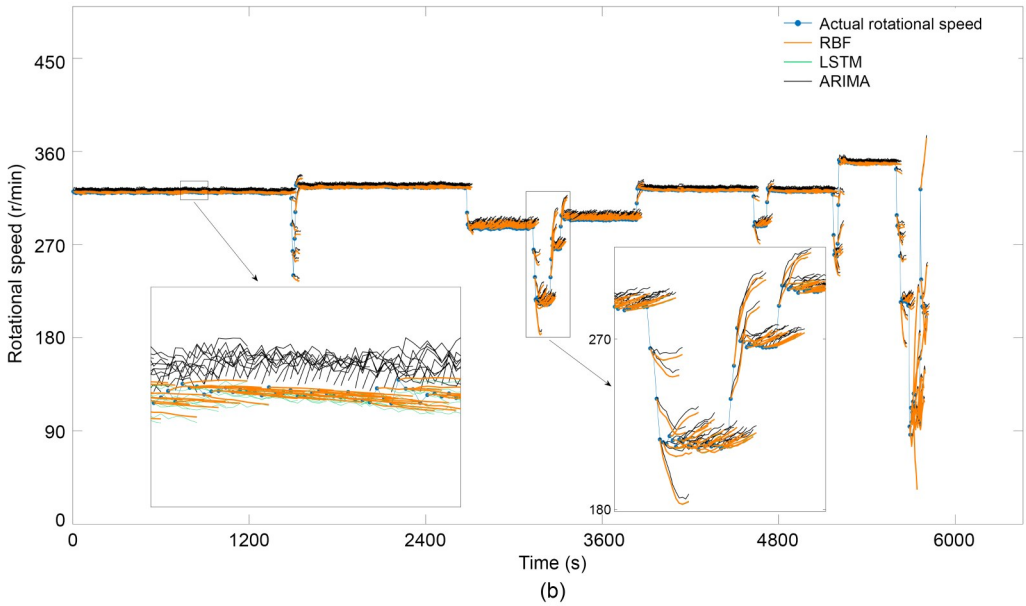

(b)

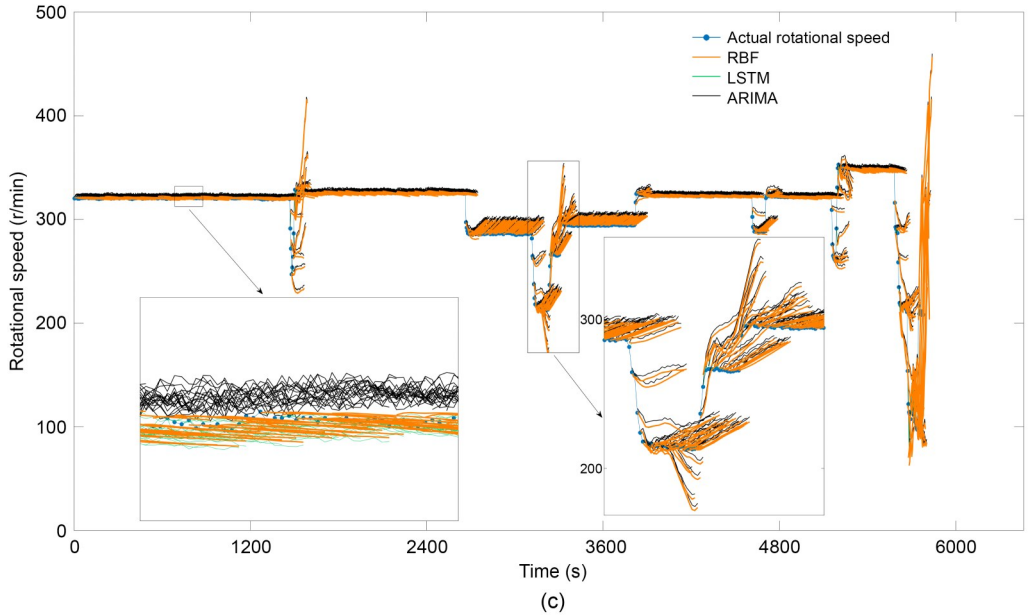

Fig. 9 Prediction results of the propulsion motor speed under different prediction lengths: (a) prediction length of 10 s; (b) prediction length of 20 s; (c) prediction length of 30 s. References to color refer to the online version of this figure

In order to further validate the effectiveness of the RBF model, a comparative analysis of the prediction results with LSTM and ARIMA is conducted, as shown in Table 2. The results demonstrate that the RBF model exhibits a significant advantage with regard to prediction accuracy, computational efficiency, and model complexity. In terms of prediction accuracy, the root mean square error (RMSE) and R^2 of the RBF model are comparable to LSTM, and are even slightly lower than LSTM under certain prediction durations. However, the RBF model significantly outperforms ARIMA in terms of computational efficiency. The training time and inference time of the RBF model are lower than those of LSTM, making it particularly suitable for scenarios with more demanding real-time requirements. A balanced assessment across the dimensions of prediction accuracy, real-time performance, and implementation complexity reveals the RBF model's suitability for ship energy management applications.

Table 2 Errors at different prediction lengths

Prediction length (s)	Method	Time (s)	RMSE	R^2
10	RBF	991.73	1.2360	0.9807
	LSTM	1617.65	1.2232	0.9821
	ARIMA	756.10	1.8914	0.9538
20	RBF	1871.60	2.4707	0.9213
	LSTM	2704.26	2.4916	0.9131
	ARIMA	1417.83	2.7325	0.8847
30	RBF	2858.75	3.5985	0.8280
	LSTM	4316.49	3.8142	0.8076
	ARIMA	2237.60	4.2733	0.7631

Furthermore, a prediction of the fuel consumption of the vessel is made using the RBF multivariate time series prediction model, and the results are shown in Fig. S4 of the ESM. A comparison of the prediction results for propulsion motor speed reveals a negative correlation between specific fuel consumption and propulsion motor speed. Specifically, a reduction in propulsion motor speed is associated with an increase in specific fuel consumption. This suggests that the current propulsion motor speed is not the most economically efficient setting, and that further optimization is possible.

4.2 MPC vessel speed optimization

The navigational environment, including wind speed and water depth, constantly changes, impacting propulsion power demand, resistance, and fuel consumption. To analyze the influence of the environment on fuel use, we assess the relative importance of such factors in fuel consumption prediction. As shown in Fig. S5 of the ESM, propulsion motor speed has the most significant impact (0.482), followed by wind speed (0.162), water flow rate (0.157), water depth

(0.131), and wind direction (0.122). Thus, we choose to prioritize optimizing motor speed to adapt to environmental changes, rather than analyzing each variable's direct impact on navigation speed.

Using the upper-level speed optimization model based on the navigational environment, the segment from Yichang to Fengdu is selected for simulation analysis. The optimized propulsion motor speed obtained using the MPC method is compared with the conventional segmented optimization method and historical speed data in Fig. 10. We can observe that the historical rotational speed of the propulsion motor remains stable for most of the time, but exhibits significant fluctuations in certain periods. The maximum rate of change is 132 r/(min·s), and these rapid variations accelerate the wear and tear on the internal mechanical components of the propulsion motor, induce abrupt temperature fluctuations, and impose stress on the ship's power grid. Over time, these effects can compromise the reliability and lifespan of the motor and negatively impact the stability of the vessel.

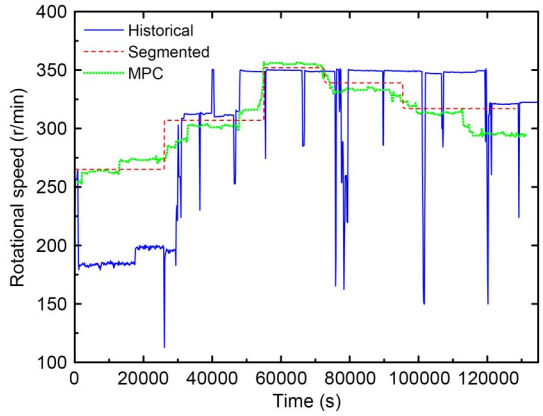

Fig. 10 Rotational speeds of propulsion motor before and after optimization by different methods

The optimization results of the conventional segmented optimization method remain constant within each predefined segment, leading to stepwise changes in rotational speed. This method divides the voyage into five segments based on the navigational environment using a clustering algorithm, assigning fixed rotational speeds of 268 r/min, 310 r/min, 355 r/min, 342 r/min, and 320 r/min, respectively. The maximum rate of change in rotational speed between adjacent segments reaches 45 r/(min·s). Although this method reduces the rate of change compared to actual speed fluctuations, it still introduces abrupt transitions that impact the propulsion motor during segment switches. Additionally, because the method assumes a constant navigation environment within each segment, it cannot promptly respond to real-time variations in external factors such as wind speed and water resistance. Consequently, sudden increases or decreases in rotational speed occur, reducing control accuracy and potentially increasing fuel consumption. Therefore, under complex navigational conditions, the conventional segmented optimization method has significant limitations in maintaining smooth and adaptive speed control.

In contrast, the MPC optimization method dynamically adjusts the rotational speed by predicting changes in the navigation environment in real time and applying a rolling optimization strategy. The rotational speed curve obtained using the MPC method is continuously smooth, with the maximum rate of change reduced to 20 r/(min·s), effectively minimizing the frequency of abrupt speed fluctuations. This enhanced dynamic adaptability allows the MPC method to better accommodate environmental variations such as wind speed and water depth, leading to a significant reduction in both the fuel consumption and EEOI. Moreover, the gradual transitions in rotational speed mitigate mechanical wear on the propulsion motor and reduce disturbances to the ship's power grid, thereby improving motor stability and extending its operational lifespan.

The optimization results of the various methods are presented in Table 3. To improve the credibility of the results, we statistically verify the energy saving ratio and the EEOI reduction rate. Through multiple simulation calculations, the mean value and 95% confidence interval of the energy saving ratio and the EEOI reduction rate are obtained. The results show that compared to the actual speed of the propulsion

Table 3 Effectiveness of different optimization methods

Item	Sailing time (s)	Degree of optimization	EEOI	Degree of optimization
Historical sailing rotational speed	134732		0.135188	
Segmented rotational speed optimization	128249	4.90%	0.129314	4.34%
MPC rotational speed optimization	131255	2.58%	0.119587	11.54%

motor, the average sailing time reduction after adopting the traditional piecewise speed optimization is 4.90%, with a 95% confidence interval of [4.58%, 5.22%], and the average reduction in EEOI is 4.34%, with a 95% confidence interval of [4.10%, 4. 58%]; the mean value of the sailing time reduction after MPC speed optimization is 2.58%, with a 95% confidence interval of [2.29%, 2.87%], and the mean value of the EEOI reduction is 11.54%, with a 95% confidence interval of [11.13%, 11.95%]. Overall, it is demonstrated that the proposed MPC speed optimization method can significantly reduce the EEOI and voyage time of the target ship during navigation.

4.3 Equivalent fuel consumption minimization strategy based on condition adaptation

Fig. 11 shows the power demand of the vessel following the optimization of the upper MPC rotational speed. It can be observed that the power demand of the vessel during this voyage can be categorized into three distinct groups: low, medium, and high. Furthermore, the overall trend appears to align with that of the optimized rotational speed of the propulsion motor.

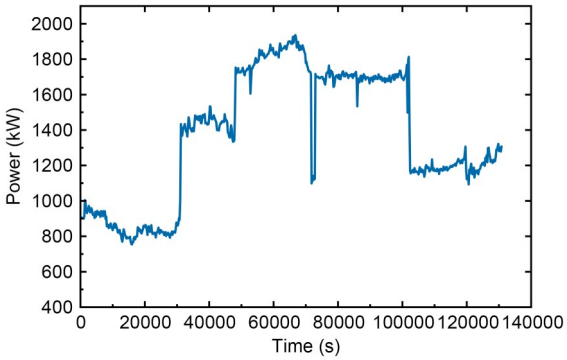

Fig. 11 Vessel power requirements

The output power of the target vessel diesel generator and supercapacitor for different equivalence factors in the ECMS is shown in Fig. S6 of the ESM. Fig. S6 shows that when the equivalence factor s=0.1, the supercapacitor operates for a longer duration than when s=6. Furthermore, the supercapacitor's operational time initially increases and then decreases with increasing s. The outcomes of the different ECMS energy management strategies are largely similar. When the equivalence factor $s \geqslant 6$, the results based on the ECMS energy management strategy are essentially identical. At this point in time, the vessel is primarily driven by the diesel generator, with less reliance on supercapacitors. This is due to the high costs associated with charging and discharging the supercapacitor, the high equivalent fuel consumption, and the relatively stable output power of the supercapacitor, which is only apparent in the initial stage. It thus follows that the selection of the target vessel equivalence factor must satisfy the following conditions:

$$s_{\min} \leqslant s \leqslant s_{\max}, \tag{33}$$

where $s_{\min}$=0.1, and $s_{\max}$=6.

This paper presents a comparative analysis of the effects of three distinct energy management strategies: the rule-based energy management strategy, the fixed-equivalence-factor ECMS strategy, and the proposed adaptive A-ECMS strategy. The initial SOC of the supercapacitor is set to 0.6 under all three strategies, while the initial value of the equivalence factor for the operating condition-adaptive A-ECMS strategy is set to a moderate value, s_0=3.

Fig. S7 of the ESM shows the fuel consumption of the vessel when the equivalence factor is within the range of [0.1, 5] for the ECMS strategy with a fixed equivalence factor. It is evident that when the equivalence factor is 3, the fuel consumption of the vessel under the ECMS strategy is the lowest. Therefore, the value of the fixed equivalence factor is taken as 3.

Fig. 12 shows the impact of varying strategies on the power output and supercapacitor SOC of each energy source in the vessel. In Figs. 12a, 12c, and 12e, the blue and orange lines represent the output power of engine No. 1 and engine No. 2, respectively. The green line represents the output power of the supercapacitor, and the red line represents the power demand of the vessel. Figs. 12b, 12d, and 12f illustrate the variations in supercapacitor SOC under different strategies.

As illustrated in Fig. 12a, the adoption of a rule-based energy management strategy results in the continuous operation of the No. 1 diesel generator, with minimal output power fluctuations that remain within the optimal range. Conversely, the No. 2 diesel generator initiates and terminates its operation on numerous occasions in response to fluctuations in power demand, resulting in considerable output power fluctuations. The supercapacitor is primarily operated between 30000 s and 59000 s, as illustrated in Fig. 12b,

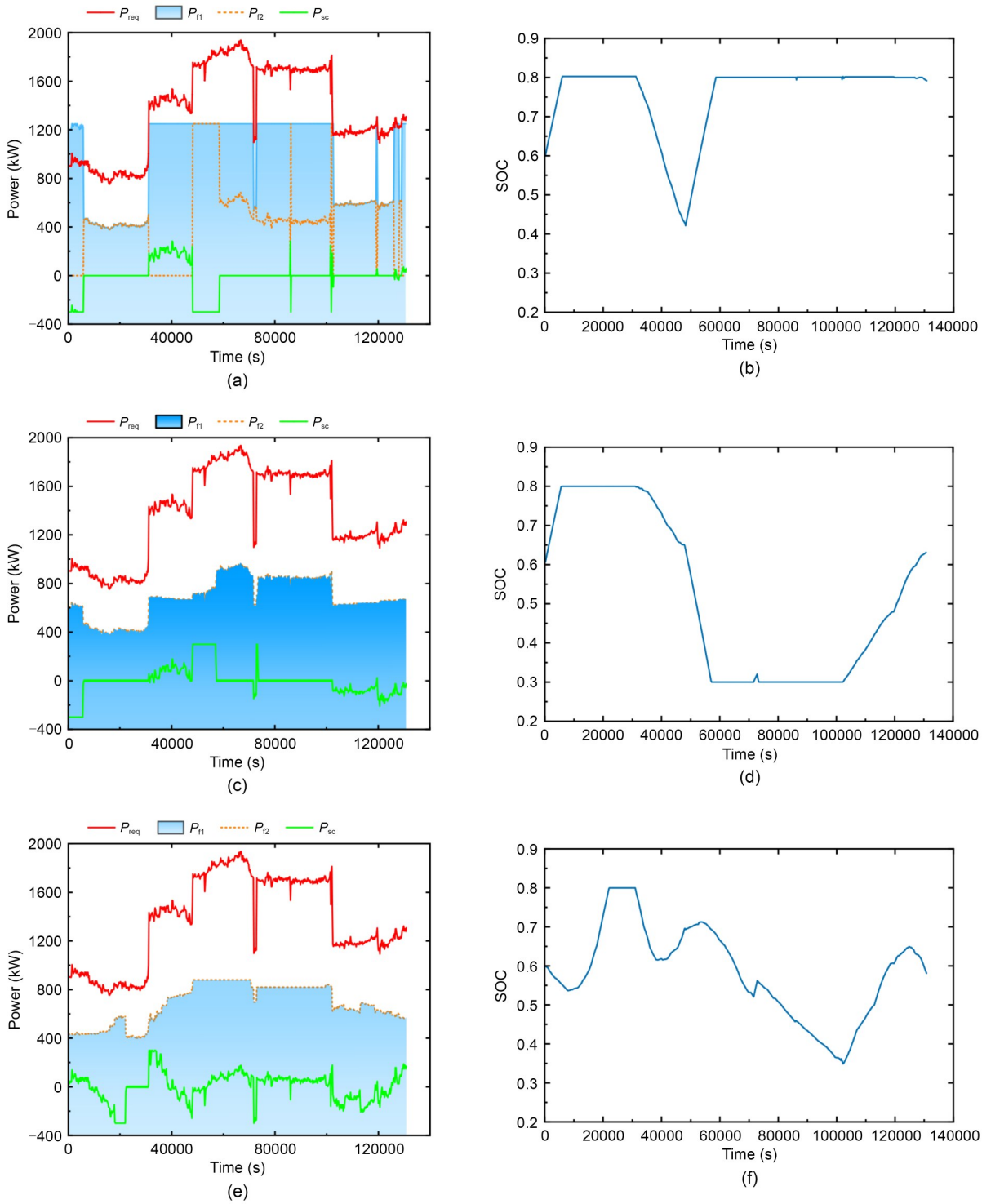

Fig. 12 Variation of powertrain output and supercapacitor SOC under different strategies: (a) power output under rule-based strategy; (b) supercapacitor SOC under rule-based strategy; (c) power output under ECMS strategy; (d) supercapacitor SOC under ECMS strategy; (e) power output under A-ECMS strategy; (f) supercapacitor SOC under A-ECMS strategy. References to color refer to the online version of this figure

and the supercapacitor SOC is predominantly maintained at 0.8.

The adoption of the fixed-equivalence-factor ECMS energy management strategy is illustrated in

Fig. 12c, which demonstrates that the supercapacitor is primarily used from 30000 s to 58000 s and 105000 s to 131000 s. These are periods during which the power demand of the vessel is considerable and exhibits considerable fluctuation. Consequently, the frequent operation of the supercapacitor can effectively mitigate the load fluctuations of the diesel generator. However, the power fluctuation of the supercapacitor is relatively smooth under other operating conditions, indicating that the value of the equivalence factor is only optimal under certain operating conditions, and not globally optimal. This reflects the drawbacks of the fixed-equivalence-factor ECMS strategy. As illustrated in Fig. 12d, the SOC of the supercapacitor exhibits fluctuations within the specified constraint range. However, the workload of the supercapacitor is relatively low in instances of low power demand and partially high power demand, resulting in a less pronounced change in SOC during these scenarios.

Fig. 12e depicts the performance of the working condition-adaptive A-ECMS energy management strategy. The output powers of the two diesel generators exhibit minimal discrepancies. During the period in which the vessel is in a high-power demand state, between 50000 s and 103000 s, the supercapacitor is utilized frequently; this flattens the diesel generator's load, and enables it to assume the role of peak shaving and valley filling. In this stage, the diesel generator's output power is markedly more even, and the instantaneous fuel consumption rate is considerably reduced. In the remaining time, the vessel is in a low-demand and medium-demand power state. When the load information is considered, one can observe that the power demand fluctuation of the vessel from 0 s to 18500 s is more pronounced than that from 106500 s to 131000 s. Consequently, the supercapacitor exhibits greater fluctuations from 0 s to 18500 s, and the supercapacitor SOC also undergoes corresponding changes. As illustrated in Fig. 12f, the supercapacitor SOC remains within the specified range, demonstrating optimal performance.

A comparative analysis of the results of the three energy management strategies reveals that the output power of the two diesel generators is significantly smoother and more similar under the ECMS and A-ECMS strategies. This contrasts with the frequent starting and stopping of diesel generator No. 2 in the rule-based strategy, and helps to reduce the fuel consumption from the diesel generator starting up. Furthermore, the supercapacitor exhibits greater fluctuations in frequency under the ECMS and A-ECMS strategies. A comparison of the supercapacitor output power under the ECMS and A-ECMS strategies reveals that the supercapacitor in ECMS operates effectively only under certain high-demand power conditions, whereas the supercapacitor in A-ECMS demonstrates superior performance in terms of smoothing the load fluctuations of the diesel generator across all scenarios. This observation highlights the effectiveness of adaptive adjustment of the equivalent factor based on operating conditions.

The final fuel consumption results of the three strategies are shown in Table S1 of the ESM. The total fuel consumption of the vessel under the rule-based strategy is 11212.547 kg, for the ECMS strategy it is 10365.334 kg, and for the A-ECMS strategy it is 10242.312 kg. The lowest fuel consumption is thus achieved by the A-ECMS strategy, which is 1.21% and 9.47% lower compared to the ECMS strategy and the logical threshold strategy, respectively. This demonstrates that the proposed adaptive condition-based equivalent fuel consumption minimization strategy A-ECMS can effectively improve the fuel economy of the vessel.

5 Conclusions

This paper proposes an optimal hierarchical control method for the management of marine vessel speed and energy, accounting for the specific navigational environment. A diesel-electric hybrid vessel is employed as a case study for simulation and analysis.

In the upper-layer speed optimization model, the proposed MPC method can reduce the total sailing time by approximately 2.58% and decrease the EEOI by approximately 11.54%. In comparison with the conventional segment optimization approach, the proposed method reduces the EEOI by about 7.5%, thereby enhancing the energy efficiency of the vessel and reducing associated time costs. Furthermore, the rotational speed of the propulsion motor obtained through the MPC voyage speed optimization method is relatively smooth, which may help extend the service life of the propulsion motor.

In the lower-layer energy management strategy model, the proposed condition-adaptive ECMS strategy reduces fuel consumption by approximately 9.47%

and 1.21% in comparison to the rule-based energy management strategy and the fixed-equivalence-factor ECMS energy management strategy, respectively. Furthermore, this strategy significantly reduces the fluctuation of the diesel generator load and decreases the number of diesel generator starts and stops.

Our novel optimal hierarchical control method reduces fuel consumption and carbon emissions, supporting the energy-saving goals put forth by the IMO and promoting green shipping practices. It enhances hybrid ship applications, improves operational efficiency, and helps meet regulations like energy efficiency existing ship index (EEXI) and carbon intensity indicator (CII), boosting market competitiveness and reducing costs.

Future research will integrate deep learning (e.g., transformers and hybrid neural networks) with sensitivity analysis to refine fuel consumption predictions in complex environments. Additionally, optimizing adjustments to the energy management and dynamic equivalence factor would further improve fuel economy and adaptability. Our strategy could also be extended to ships powered by different forms of energy, utilized for multi-energy optimization, and integrated with intelligent shipping technologies. We recommend validation through simulations and small-scale ship experiments to refine such models and confirm their effectiveness.

Acknowledgments

This work is supported by the National Natural Science Foundation of China (No. 52571367) and the Commissions Project of China (No. CBG4N21).

Author contributions

Zhe XIONG: formal analysis, investigation, writing–original draft, and data curation. Yupeng YUAN: conceptualization, methodology, writing–review & editing, resources, and supervision. Liang TONG: writing–review & editing. Jianshu CHU: investigation and resources. Boyang SHEN: writing–review & editing.

Conflict of interest

Zhe XIONG, Yupeng YUAN, Liang TONG, Jianshu CHU, and Boyang SHEN declare that they have no conflict of interest.

References

Balsamo F, Capasso C, Miccione G, et al., 2017. Hybrid storage system control strategy for all-electric powered ships. *Energy Procedia*, 126:1083-1090. https://doi.org/10.1016/j.egypro.2017.08.242

Bassam AM, Phillips AB, Turnock SR, et al., 2017. Development of a multi-scheme energy management strategy for a hybrid fuel cell driven passenger ship. *International Journal of Hydrogen Energy*, 42(1):623-635. https://doi.org/10.1016/j.ijhydene.2016.08.209

Carlton JS, 2018. Marine Propellers and Propulsion. 4th Edition. Elsevier, Amsterdam, the Netherlands.

Chen ZH, Liu YG, Zhang YJ, et al., 2022. A neural network-based ECMS for optimized energy management of plug-in hybrid electric vehicles. *Energy*, 243:122727. https://doi.org/10.1016/j.energy.2021.122727

Gao SC, Zong YH, Ju F, et al., 2024. Scenario-oriented adaptive ECMS using speed prediction for fuel cell vehicles in real-world driving. *Energy*, 304:132028. https://doi.org/10.1016/j.energy.2024.132028

Geertsma RD, Negenborn RR, Visser K, et al., 2017. Pitch control for ships with diesel mechanical and hybrid propulsion: modelling, validation and performance quantification. *Applied Energy*, 206:1609-1631. https://doi.org/10.1016/j.apenergy.2017.09.103

Guo LL, Gao BZ, Gao Y, et al., 2017. Optimal energy management for HEVs in eco-driving applications using bi-level MPC. *IEEE Transactions on Intelligent Transportation Systems*, 18(8):2153-2162. https://doi.org/10.1109/TITS.2016.2634019

Han L, Jiao XH, Zhang Z, 2020. Recurrent neural network-based adaptive energy management control strategy of plug-in hybrid electric vehicles considering battery aging. *Energies*, 13(1):202. https://doi.org/10.3390/en13010202

Hasanvand S, Rafiei M, Gheisarnejad M, et al., 2020. Reliable power scheduling of an emission-free ship: multiobjective deep reinforcement learning. *IEEE Transactions on Transportation Electrification*, 6(2):832-843. https://doi.org/10.1109/TTE.2020.2983247

Hein K, Xu Y, Wilson G, et al., 2021. Coordinated optimal voyage planning and energy management of all-electric ship with hybrid energy storage system. *IEEE Transactions on Power Systems*, 36(3):2355-2365. https://doi.org/10.1109/TPWRS.2020.3029331

Holtrop J, 1984. A statistical re-analysis of resistance and propulsion data. *International Shipbuilding Progress*, 31(363): 272-276.

Holtrop J, Mennen GGJ, 1982. An approximate power prediction method. *International Shipbuilding Progress*, 29(335): 166-170. https://doi.org/10.3233/ISP-1982-2933501

Hou J, Sun J, Hofmann HF, 2018. Mitigating power fluctuations in electric ship propulsion with hybrid energy storage system: design and analysis. *IEEE Journal of Oceanic Engineering*, 43(1):93-107. https://doi.org/10.1109/JOE.2017.2674878

Hou J, Yao DW, Wu F, et al., 2021. Online vehicle velocity prediction using an adaptive radial basis function neural network. *IEEE Transactions on Vehicular Technology*, 70(4): 3113-3122.

https://doi.org/10.1109/TVT.2021.3063483

IMO (International Maritime Organization), 2023. 2023 IMO Strategy on Reduction of GHG Emissions from Ships. IMO.

Kalikatzarakis M, Geertsma RD, Boonen EJ, et al., 2018. Ship energy management for hybrid propulsion and power supply with shore charging. *Control Engineering Practice*, 76:133-154. https://doi.org/10.1016/j.conengprac.2018.04.009

Khan MMSK, Faruque MO, Newaz A, 2017. Fuzzy logic based energy storage management system for MVDC power system of all electric ship. *IEEE Transactions on Energy Conversion*, 32(2):798-809. https://doi.org/10.1109/TEC.2017.2657327

Li YP, Wang F, Tang XL, et al., 2022. Real-time multiobjective energy management for electrified powertrains: a convex optimization-driven predictive approach. *IEEE Transactions on Transportation Electrification*, 8(3):3139-3150. https://doi.org/10.1109/TTE.2022.3158275

Liu CX, Li XY, Chen Y, et al., 2023. Real-time energy management strategy for fuel cell/battery vehicle based on speed prediction DP solver model predictive control. *Journal of Energy Storage*, 73:109288. https://doi.org/10.1016/j.est.2023.109288

Liu H, Wang YC, Gao DJ, 2021. Research on control strategy of hybrid electric ship based on minimum equivalent fuel consumption. *IOP Conference Series: Earth and Environmental Science*, 632:032029. https://doi.org/10.1088/1755-1315/632/3/032029

Liu YS, Ge YS, Tan JW, et al., 2018. Emission characteristics of offshore fishing ships in the Yellow Bo Sea, China. *Journal of Environmental Sciences*, 65:83-91. https://doi.org/10.1016/j.jes.2017.02.020

Sulligoi G, Vicenzutti A, Menis R, 2016. All-electric ship design: from electrical propulsion to integrated electrical and electronic power systems. *IEEE Transactions on Transportation Electrification*, 2(4):507-521. https://doi.org/10.1109/TTE.2016.2598078

Tian X, He R, Sun XD, et al., 2020. An ANFIS-based ECMS for energy optimization of parallel hybrid electric bus. *IEEE Transactions on Vehicular Technology*, 69(2):1473-1483. https://doi.org/10.1109/TVT.2019.2960593

UNCTAD (United Nations Conference on Trade and Development), 2022. Review of Maritime Transport 2022: Navigating Stormy Waters. United Nations Publications.

Wu P, Partridge J, Bucknall R, 2020. Cost-effective reinforcement learning energy management for plug-in hybrid fuel cell and battery ships. *Applied Energy*, 275:115258. https://doi.org/10.1016/j.apenergy.2020.115258

Xie PL, Tan S, Guerrero JM, et al., 2021. MPC-informed ECMS based real-time power management strategy for hybrid electric ship. *Energy Reports*, 7(S1):126-133. https://doi.org/10.1016/j.egyr.2021.02.013

Zahedi B, Norum LE, Ludvigsen KB, 2014. Optimized efficiency of all-electric ships by dc hybrid power systems. *Journal of Power Sources*, 255:341-354. https://doi.org/10.1016/j.jpowsour.2014.01.031

Zhang N, Ma XH, Jin LM, 2017. Energy management for parallel HEV based on PMP algorithm. The 2nd International Conference on Robotics and Automation Engineering (ICRAE), p.177-182. https://doi.org/10.1109/ICRAE.2017.8291376

Zhu JY, Chen L, Wang XF, et al., 2020. Bi-level optimal sizing and energy management of hybrid electric propulsion systems. *Applied Energy*, 260:114134. https://doi.org/10.1016/j.apenergy.2019.114134

Zhu LS, Han JG, Peng DK, et al., 2014. Fuzzy logic based energy management strategy for a fuel cell/battery/ultracapacitor hybrid ship. The 1st International Conference on Green Energy, p.107-112. https://doi.org/10.1109/ICGE.2014.6835406

Electronic supplementary materials

Table S1, Figs. S1–S7